Synthesis, characterization, and SAMs electroactivity of ruthenium complexes with sulfur containing ligands

Jackson R. de Sousa [a], Izaura C.N. Diógenes [a], Márcia L.A. Temperini [b],
Francisco A.M. Sales [a], Solange de O. Pinheiro [a], Raimundo N. Costa Filho [c],
José S. de Andrade Júnior [c], Ícaro de S. Moreira [a],*

[a] *Departamento de Química Orgânica e Inorgânica, Universidade Federal do Ceará, Cx Postal 12200, 60455-760, Fortaleza, CE, Brazil*
[b] *Instituto de Química, Universidade de São Paulo, Cx Postal 26077, 05513-970, São Paulo, SP, Brazil*
[c] *Departamento de Física, Universidade Federal do Ceará, Cx Postal 6030, 60451-970, Fortaleza, CE, Brazil*

Abstract

The vibrational and ^{1}H NMR data hints that the coordination of the 2,2′-dithiodipyridine (2-pySS) ligand to the $[Ru(CN)_5]^{3-}$ metal center occurs through the sulfur atom instead of the nitrogen atoms which is usually observed for *N*-heterocyclic ligands. Electrochemical results show that this coordination mode implies an additional thermodynamic stabilization of the Ru^{II} over Ru^{III} oxidation state due to a relative stronger π-back-bonding interaction with the empty low-lying dπ orbitals of the sulfur atom. Computational data reinforce the experimental results showing that the 2-pySS Lewis base centers are located on the sulfur atoms. Ligands containing only sulfur atoms as coordination sites (2,2′-dithiodipyridine *N*-oxide (2-pySSNO), 1,4-dithiane (1,4-dt), and 2,6-dithiaspiro[3.3]heptane (asp)) were also coordinated to the $[Ru(CN)_5]^{3-}$ metal center to undoubtedly correlate the electrochemical results with the ligand coordination atom. Among the synthesized compounds, the $[Ru(CN)_5(1,4-dt)]^{3-}$ and $[Ru(CN)_5(asp)]^{3-}$ complexes showed to be able to form self-assembled monolayers (SAMs) on gold. These SAMs, which were characterized by SERS (surface-enhanced Raman scattering) spectroscopy, successfully assessed the heterogeneous electron transfer reaction of the cytochrome *c* metalloprotein in physiological medium.
© 2007 Elsevier B.V. All rights reserved.

Keywords: Sulfur containing ligands; Ruthenium complexes; Cyclic voltammetry; Computational simulation; SAM; Cytochrome *c*

1. Introduction

Understanding the nature of the metal–sulfur bond is of great importance due to the involvement of both metal ions and sulfur ligands in biological systems [1–3]. For instance, the thermodynamic stabilization of the cytochrome *c* metalloprotein keeps a remarkable dependence on the oxidation state of iron ion. The stability gain of cyt *c* (Fe^{II}) compared with cyt *c* (Fe^{III}) is assigned to the π-back-bonding interaction from the metal to the methionine residue. Although not definitely established, this interaction may

be addressed to the capability of the methionine sulfur atom to use the low-lying empty dπ orbitals [4]. Also it may arise from the softness of the methionine sulfur [5] that favors the interaction to the soft Fe^{II} ion. Moreover, the coordination of sulfur containing ligands through the sulfur atom strongly affects the redox potentials of transition metal ions [4]. For instance, an increase in the reduction potentials of the $Ru^{III/II}$ couple for $[Ru(NH_3)_5L]^{2+}$ type complexes, where L = sulfur donor ligands instead of nitrogen or oxygen, is observed [4]. Similar trends in redox potentials were also observed for a series of $[Fe(CN)_5L]^{2+}$ type complexes [6], and ruthenium and osmium porphyrin complexes [7]. The stabilization of M^{II} over M^{III} oxidation state upon coordination to a sulfur donor ligand seems to

---

* Corresponding author.
  E-mail address: icarosm@dqoi.ufc.br (Ícaro de S. Moreira).

be so great that, even in complexes with π-donor ligands, a positive potential shift is observed for the $M^{III/II}$ related process. In fact, the [Ru(Cl)$_2$(dppb)(1,4-dt)] complex, where dppb = 1,4-bis(diphenylphosphine)butane, 1,4-dt = 1,4-dithiane, the half-wave formal potential ($E_{1/2}$) assigned to the $Ru^{III/II}$ redox process shifts for about 100 mV in the positive direction in relation to similar compounds in which the 1,4-dt ligand is replaced by a *N*-heterocyclic species [8].

Although the dependence of the redox potentials of transition metal complexes on the nature of the ligand donor atom is well discussed in the literature for a series of ruthenium ammine and ironpentacyano complexes, [6,9–11], there are a few [Ru(CN)$_5$L]$^{n+}$ type systems, where L = sulfur donor ligand, displaying a range of redox data enough for systematic correlations. Aiming to contribute to the understanding of the additional stabilization of the reduced state of metal ions upon coordination to sulfur containing ligands, [Ru(CN)$_5$(L)]$^{3-}$ type complexes, L = 2,2′-dithiodipyridine (2-pySS), 2,2′-dithiodipyridine *N*-oxide (2-pySSNO), 1,4-dithiane (1,4-dt), and 2,6-dithiaspiro[3.3]heptane (asp), were synthesized and characterized. The planar representation of these ligands and the [Ru(CN)$_5$(2-pySS)]$^{3-}$ complex are illustrated in Chart 1. The representation of the 4,4′-dithiodipyridine (4-pySS) molecule is also presented for comparative purposes.

Computational simulations were performed aiming to theoretically explain the affinity of the ruthenium central atom toward specific atoms of the ligands.

Additionally, based on the well known affinity of sulfur containing molecules to gold [12], self-assembled monolayers (SAMs) were formed with the synthesized complexes. The electroactivity of these SAMs, which were characterized by SERS (surface-enhanced Raman scattering) spectroscopy, was evaluated by using the cytochrome *c* metalloprotein as probe molecule.

2. Results and discussion

The characterization of the [Ru(CN)$_5$(2-pySS)]$^{3-}$ complex was carried out by high performance liquid chromatography (HPLC), elemental analysis, proton nuclear magnetic resonance (^{1}H NMR), electronic, infrared, and Raman spectroscopies, and cyclic voltammetry.

By accounting for the different chemical properties of the starting materials that in most of cases implies in different interactions with a given chromatographic column, the retention times acquired from the HPLC chromatograms of the [Ru(CN)$_5$(2-pySS)]$^{3-}$ complex (4.72 min) and the 2-pySS ligand (9.16 min), and the [Ru(CN)$_6$]$^{4-}$ starting complex (2.03 min), suggest that the complex was isolated with high purity level. The elemental analysis results reinforce this assignment and are consistent with the
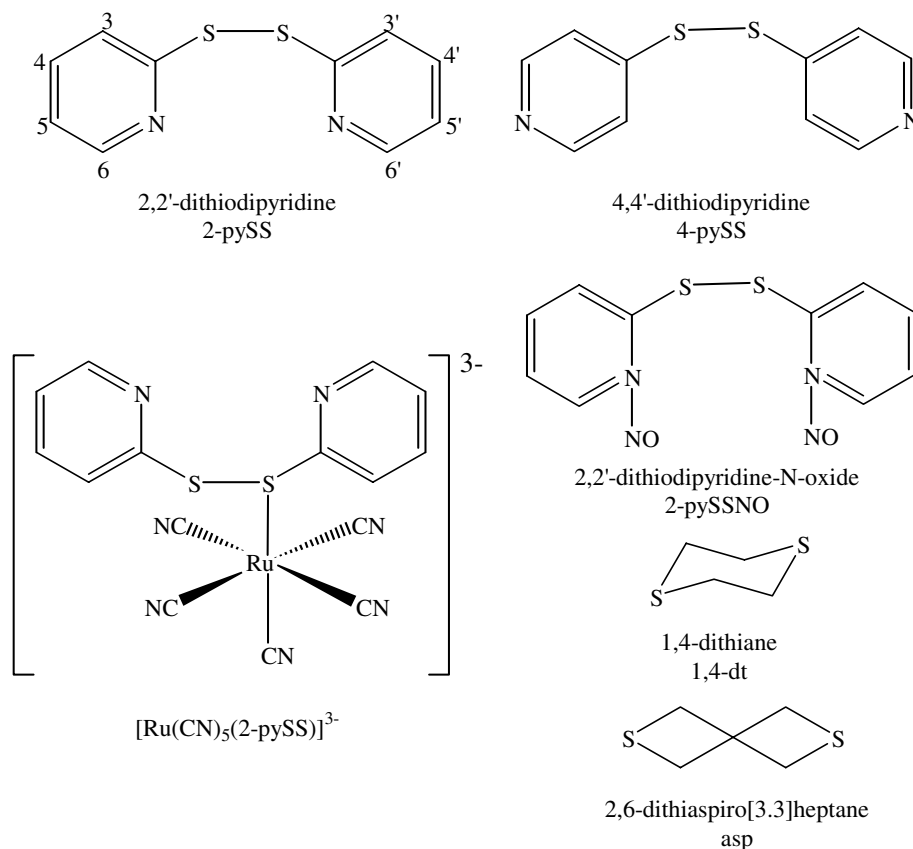

Chart 1. Planar representation of the 2-pySS, 4-pySS, 2-pySSNO, 1,4-dt, and asp ligands, and the [Ru(CN)$_5$(2-pySS)]$^{3-}$ complex.

formulation specified for the complexes as $K_3[Ru(CN)_5(L)] \cdot 3H_2O$, where L = 2,2′-dithiodipyridine (2-pySS) (1), 2,2′-dithiodipyridine N-oxide (2-pySSNO) (2), 1,4-dithiane (1,4-dt) (3), and 2,6-dithiaspiro[3.3]heptane (asp).

2.1. NMR

Based on the ^{1}H NMR spectrum of the 2,2′-bipyridine [13], the signals observed in the spectrum of the 2-pySS ligand free of coordination were assigned as: δ 8.47 (H$_{6/6'}$, ddd; $J_1 = 4.8$ Hz, $J_2 = 1.8$ Hz, $J_3 = 1.0$ Hz), δ 7.77 (H$_{4/4'}$, ddd; $J_1 = 8.1$ Hz, $J_2 = 7.4$ Hz, $J_3 = 1.8$ Hz), δ 7.66 (H$_{3/3'}$, td; $J_1 = 8.1$ Hz, $J_2 = 1.0$ Hz, $J_3 = 1.0$ Hz) and δ 7.24 ppm (H$_{5/5'}$, ddd; $J_1 = 7.4$ Hz, $J_2 = 4.8$ Hz, $J_3 = 1.0$ Hz). These assignments are corroborated by the splitting constants observed between the adjacent protons. The ^{1}H NMR analysis of the $[Ru(CN)_5(2\text{-pySS})]^{3-}$ complex was performed in a comparative form by evaluating the chemical shifts of the 2,2′-dithiodipyridine free ligand and upon coordination to the $[Ru(CN)_5]^{3-}$ metal center. An interesting feature of this spectrum is the chemical shift presented by the signals assigned to the H$_6$ and H$_3$ atoms of the 2-pySS ligand (Chart 1). Comparatively to other similar systems in which the sixth ligand is a N-heterocyclic species [14], an unusual downfield shift is observed. For the free ligand, the H$_6$ and H$_3$ hydrogen signals are observed at δ 8.47 and 7.66 ppm, respectively. Upon coordination to the ruthenium metal center, a shift to δ 9.13 and 7.97 ppm is observed, respectively. This behavior is assigned to the coordination of the 2-pySS ligand through a sulfur atom instead of the nitrogen atom as is observed for the coordination of the 4,4′-dithiodipyridine [11] to the $[Ru(CN)_5]^{3-}$ metal center. In fact, downfield shifts of signals assigned to the atoms close to the coordination site are frequently observed for N-heterocyclic ligands upon coordination to metal centers because of the electronic density delocalization in consequence of the π-back-bonding interaction. The relatively higher shift observed for the hydrogen atoms in the vicinity of the 2-pySS sulfur atoms is believed to be due to the contribution of the empty dπ orbitals of sulfur, which enhances the π-back-bonding interaction thus inducing a higher electronic density delocalization.

Six signals are also presented in the ^{1}H NMR spectrum of the $[Ru(CN)_5(2\text{-pySS})]^{3-}$ complex: four of which are assigned to the protons of the remote pyridine ring at δ 8.45 (H$_6'$, ddd; $J_1 = 4.8$ Hz, $J_2 = 1.8$ Hz, $J_3 = 1.0$ Hz), δ 7.62 (H$_3'$), δ 7.31 (H$_4'$), δ 7.74 ppm (H$_5'$) and the other two at δ 7.52 and 7.41 ppm to the H$_4$ and H$_5$ protons, respectively.

2.2. Vibrational spectra

The vibrational infrared (IR) and Raman spectra of the $K_3[Ru(CN)_5(2\text{-pySS})] \cdot 3H_2O$ complex is dominated by the axial and equatorial cyanide stretching vibrations, $v(CN)_{ax}$ and $v(CN)_{eq}$, at 2100 and 2068 cm^{-1}, respectively [15].

Accounting for the shift of about 70 cm^{-1} to higher frequency that is currently observed for Ru^{III} analogue complexes [16,17], the $v(CN)_{ax}$ and $v(CN)_{eq}$ frequency values hint that the ruthenium metal center is in the reduced Ru^{II} state. The most prominent features of these spectra are distinguished in Table 1, along with the vibrational data of the 2-pySS free ligand for comparative purposes.

The SS stretching vibration ($v(SS)$) is observed as a prominent line at 504 cm^{-1} in the Raman spectrum of the $K_3[Ru(CN)_5(2\text{-pySS})] \cdot 3H_2O$ complex. Comparatively to the 2-pySS free ligand, the downshift of this vibration from 545 to 504 cm^{-1} in the Raman spectrum of the complex suggests that the coordination occurs through one of the sulfur atoms of the ligand. Also, the observation of this mode in the Raman spectrum of this complex indicates that the SS bridge was not broken upon coordination. Additionally, the presence of the NH deformation vibration ($\delta(NH)$) at 1230 cm^{-1} in the spectra of the complex reinforces the assignment of the sulfur atom as the coordination site of the 2-pySS ligand.

2.3. Electrochemical data

All the isolated complexes presented a well behaved and typically reversible voltammogram [23] with the $E_{1/2}$ values and the difference between the anodic and cathodic peak potentials, ΔE_p, independent of the scan rate from 50 to 350 mV s^{-1}. Also, in all cases, a linear dependence of the cathodic peak current (i_{pc}) with the square-root ($v^{1/2}$) of the scan rate was observed. These results indicate that the Ru$^{III/II}$ redox process of the isolated complexes are reversible, one-electron transfer, and diffusion-controlled. Comparatively to the $[Ru(CN)_6]^{3-}$ starting material ($E_{1/2} = 0.70$ V) [24], the $E_{1/2}$ values of the synthesized compounds

Table 1
Vibrational IR and Raman frequencies, cm^{-1}, of the 2-pySS and $K_3[Ru(CN)_5(2\text{-pySS})] \cdot 3H_2O$ compounds

2-pySS		$K_3[Ru(CN)_5$ (2-pySS)$] \cdot 3H_2O$		Assignment [15–22]
IR	Raman	IR	Raman	
	545		504	$v(SS)$
		522		$v(Ru–CN)$
613	616		620	$\beta(CCC)$
714	717		720	$v(CS)/\beta(CCC)$
758		766		$\gamma(CH)$
984	985	993	993, 1011	Ring breathing
1042, 1082	1044, 1088	1111, 1285		$\beta(CH)$
1113, 1146	1157, 1140			
1230	1230		1230	$\delta(NH)$
1414, 1445, 1568	1429	1418, 1450, 1574	1560	$v(C=C + C=N)$
1655			1647	$v(C=C)$
		2068, 2100	2068, 2100	$v(CN)_{ax}$ and $v(CN)_{eq}$

Table 2
$E_{1/2}$ values (V vs Ag|AgCl|Cl$^-$) for the Ru$^{III/II}$ redox process of some [Ru(CN)$_5$L]$^{3-}$ complexes (L = N- and S-donor ligands)

L = N-donor	$E_{1/2}$	Reference	L = S-donor	$E_{1/2}$	Reference
pySSpy	0.75	[13]	1,4-dt	0.91	This work
4-bpy*	0.50	[24]	2-pySSNO	0.92	This work
pz	0.72	[25]	2-pySS	0.92	This work
pyS	0.78	[26]	asp	0.90	This work

* 4-bpy = 4,4′-bipyridine.

indicate the stabilization of the ruthenium metal center in the reduced, Ru^{II}, state. The electrochemical data obtained for the [Ru(CN)$_5$(2-pySS)]$^{3-}$, [Ru(CN)$_5$(1,4-dt)]$^{3-}$, [Ru(CN)$_5$(2-pySSNO)]$^{3-}$, and [Ru(CN)$_5$(asp)]$^{3-}$ complexes as well as for some related compounds for comparative purpose are shown in Table 2.

As can be seen from the data displayed in Table 2, the nature of the N-donor ligand does not meaningfully affect the $E_{1/2}$ values for the ruthenium pentacyano complexes, except for the 4-bpy ligand. These results are explained based on the model proposed by Johnson and Shepherd [25] in which little mixing is expected to occur between the metal and the sixth ligand orbitals in the [M(CN)$_5$L]$^{3-}$ series (M = Fe, Ru) because of the strong stabilization of the metal dπ orbitals furnished by the cyanide groups. For the [Ru(CN)$_5$(1,4-dt)]$^{3-}$, [Ru(CN)$_5$(2-pySSNO)]$^{3-}$, and [Ru(CN)$_5$(asp)]$^{3-}$ complexes, however, a strong shift toward positive potential values is observed comparatively to the [Ru(CN)$_6$]$^{4-}$ complex. As the 1,4-dt, 2-pySSNO, and asp ligands have only sulfur donor atoms, the stabilization of the ruthenium metal atom in the reduced state must be related to the participation of the sulfur low-lying empty dπ orbitals in a π-back-bonding interaction. By accounting for this effect, the $E_{1/2}$ value calculated for the [Ru(CN)$_5$(2-pySS)]$^{3-}$ complex (0.92 V) strongly suggests that the 2-pySS ligand is coordinated to the ruthenium metal atom through the sulfur atom. In fact, the effective capability of sulfur containing ligands in stabilizing the Ru^{II} over Ru^{III} oxidation state has been observed for [Ru(NH$_3$)$_5$L]$^{2+}$ type complexes [4,25,24,27]. For instance, the $E_{1/2}$ value for the Ru$^{III/II}$ redox process of the [Ru(NH$_3$)$_5$(DMSO)]$^{2+}$ complex is observed at 0.78 and −0.22 V vs when the DMSO ligand is S and O-bonded, respectively [25,28].

The electrochemical results reinforce the anticipated NMR and vibrational spectroscopic suggestions: the 2-pySS ligand is coordinated to the ruthenium metal center through the sulfur atom.

2.4. Computational data

Molecular simulations are well suited to study electronic density and provide molecular-level information concerning the interaction of a metal with a specific site of a given ligand thus allowing the understanding of the related chemical reactivity. In this way, the electrostatic potential (EP) has been widely believed to explain the interaction between

molecules as well as the molecular recognition process itself.

The EP at an observation point r called $\varphi(r)$, is defined by the work done to bring a unit charge from infinity to that desired point of observation. The energy interaction between a charge q located at r and a molecule is equal to $q\varphi(r)$. However, the EP at the charge location is a contribution from the nuclei and electrons. This is the main difference from the electron density approach, which reflects only the electronic distribution. Because electrostatic forces are the basic ones generating long range interactions in molecules, the calculation of EP is necessary in order to better understand molecular interactions [29]. The EP is quantum mechanically defined in terms of the spatial coordinates of the charges on the nuclei and the electronic density function $\rho(r)$ of the molecule. The EP due to the nuclei contribution is given by

$$\phi_{\text{nuclei}}(r) = \sum_{A=1}^{M} \frac{Z_A}{|r - R_A|}, \qquad (1)$$

whereas the electronic contribution obtained from the integration in the whole space of the electronic density is given by

$$\phi_{\text{elec}}(r) = -\int \frac{\mathrm{d}r'\rho(r)}{|r' - r|}. \qquad (2)$$

Therefore, the total electrostatic potential is

$$\phi(r) = \phi_{\text{elec}}(r) + \phi_{\text{nuclei}}(r). \qquad (3)$$

Since the EP is the net result of the opposing effects of nuclei and electrons, electrophiles will be guided to the regions of a molecule where the EP is most negative. Negative electrostatic potential (nEP) corresponds to an attraction of the proton by the concentrated electron density in the molecules, i.e. lone pairs, π-bonds, etc. On the other hand, positive electrostatic potential (pEP) corresponds to repulsion of the proton by the atomic nuclei in regions where low electron density exists and the nuclear charge is not completely shielded.

The nEP, which reflects the electronic density localization on the molecule, was comparatively evaluated for the 2-pySS and 4-pySS ligands since, for the latter, the coordination undoubtedly occurs through the nitrogen atom [11]. Figs. 1 and 2 show the EP for the 2-pySS and 4-pySS molecules. Schematic depictions of the stick drawing of the complexes showing the most probable coordination site of the 2-pySS and 4-pySS molecules as indicated by the electrostatic potential studies are also presented in Figs. 1 and 2.

The computational simulation results provide additional evidence on the coordination mode of the 2-pySS ligand. For this species, the nEP was achieved to be localized over the central part of the molecule, as illustrated in Fig. 1. Thus, it can be inferred that the 2-pySS ligand has Lewis base centers on the sulfur atoms. On the other hand, as can be seen in Fig. 2, the nEP for the 4-pySS
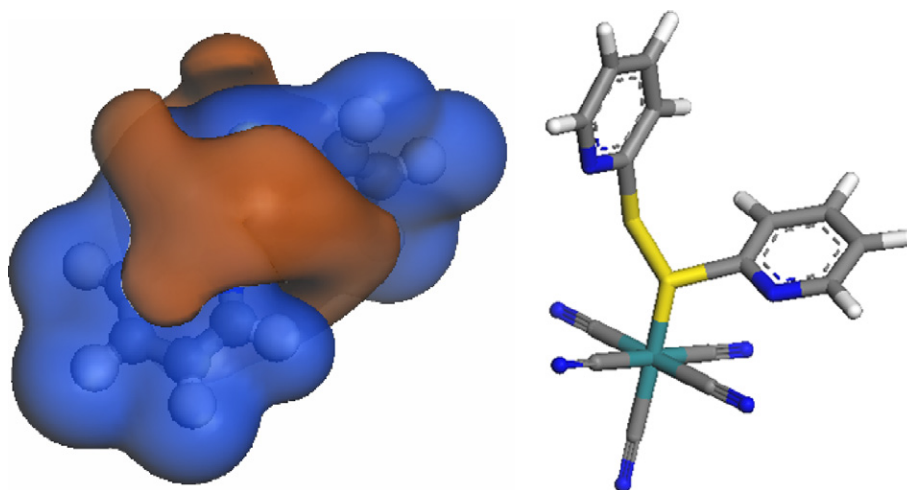
Fig. 1. Schematics of 2-pySS (ball and stick) molecule showing the nEP (red area) and the pEP (blue area) contours, and [Ru(CN)$_5$(2-pySS)] complex (stick). (For interpretation of colour representation in this figure legend the reader is referred to the web version of this article.)
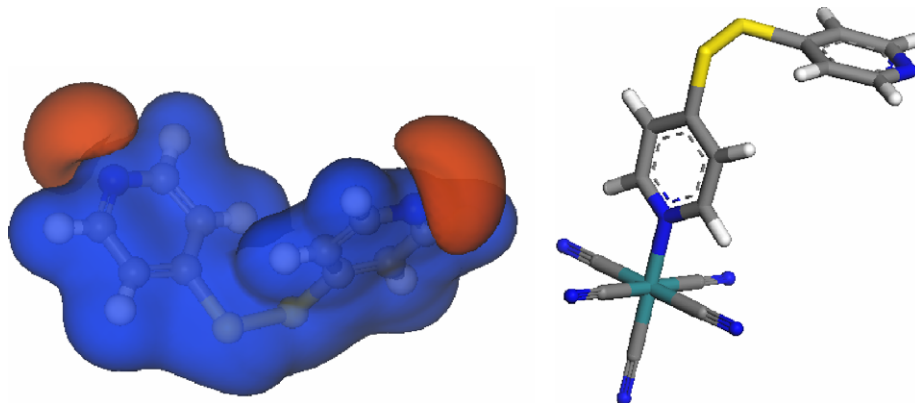

Fig. 2. Schematics of 4-pySS (ball and stick) molecule showing the nEP (red area) and the pEP (blue area) contours, and [Ru(CN)$_5$(4-pySS)] complex (stick). (For interpretation of colour representation in this figure legend the reader is referred to the web version of this article.)

ligand is localized on the nitrogen atoms. This result is in agreement with experimental data obtained by cyclic voltammetry and NMR, and vibrational spectroscopies. Therefore, based on these theoretical data, the preferential interaction of the ruthenium metal ion toward the sulfur and nitrogen atoms in the 2-pySS and 4-pySS ligands, respectively, can be justified. Also, the suggestion of the Lewis base centers explains the affinity of the Ru^{II} atom, a soft acid, to the sulfur and nitrogen atoms in the 2-pySS and 4-pySS ligands, respectively, according to the Pearson classification [5]. This affinity is schematically represented by the stick drawing of the [Ru(CN)$_5$(2-pySS)] and [Ru(CN)$_5$(4-pySS)] complexes illustrated in Figs. 1 and 2, respectively.

2.5. SAMs characterization

Since we have reported a series of Fe^{II} and Ru^{II} metal complexes with ligands containing sulfur as donor atoms [26,30–32] that form SAMs able to assess the electrochemistry of cyt *c* metalloprotein, attempts were made aiming to modify gold polycrystalline surfaces with the synthesized complexes. The characterization of the gold modified surfaces was performed by SERS spectroscopy. Successful results, however, were only obtained for the surfaces modified with [Ru(CN)$_5$(1,4-dt)]$^{3-}$ complex. For the gold surface modified with the [Ru(CN)$_5$(asp)]$^{3-}$ complex, the SERS spectrum was not acquired to avoid the contamination of the laboratory. For the [Ru(CN)$_5$(2-pySS)]$^{3-}$ and [Ru(CN)$_5$(2-pySSNO)]$^{3-}$ compounds, SAMs formation was not observed. This conclusion is based on the fact that the SERS spectra acquired for the gold electrodes immersed in the respective solutions did not show the characteristic peaks of the complexes, even after 48 h of immersion. This result is assigned to the steric hindrance and the protection of the sulfur atoms in the 2-pySS and 2-pySSNO moieties, respectively.

The SERS spectrum obtained for the gold electrode after 15 min of immersion in a 20 mmol L^{-1} aqueous solution of the [Ru(CN)$_5$(1,4-dt)]$^{3-}$ complex is illustrated in Fig. 3. The normal Raman spectrum of the complex in the solid state is also presented for comparative purposes.
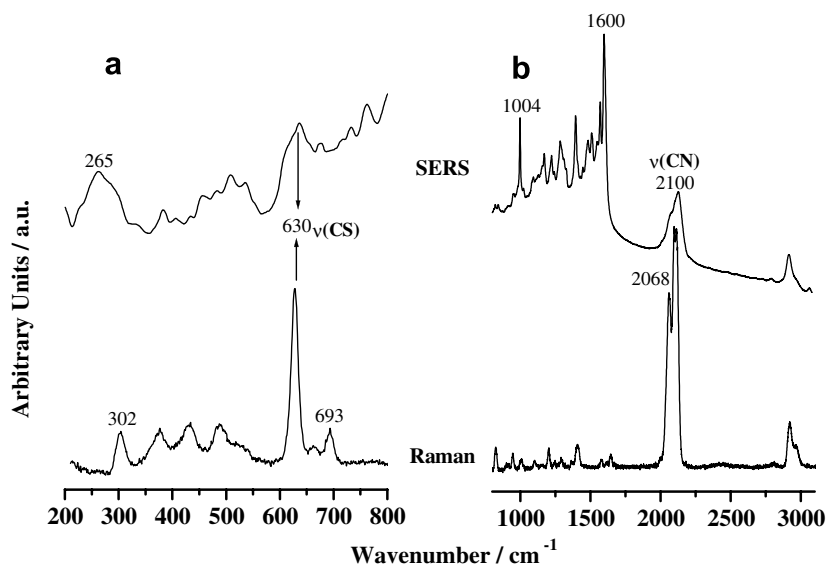
Fig. 3. Normal Raman (bottom curves) and SERS spectra (top curves) of the $K_3[Ru(CN)_5(1,4-dt)] \cdot 3H_2O$ complex in the solid state and adsorbed on gold, respectively. (a) Presented with magnification of 10× in relation to (b).

For the sake of clarity, the SERS and normal Raman spectra were separated in two regions, from 200 to 800 cm^{-1} (Fig. 3a) and from 800 to 2250 cm^{-1} (Fig. 3b). Yet, the SERS spectrum of Fig. 3a is presented with a magnification of 10× in relation to that of Fig. 3b.

The strongest signals observed in the normal Raman spectrum of the $K_3[Ru(CN)_5(1,4-dt)] \cdot 3H_2O$ complex are assigned to the $v(CN)_{ax}$ and $v(CN)_{eq}$ of the cyanide groups at 2100 and 2068 cm^{-1} [15], respectively, and the $v(CS)$ at 630 cm^{-1} [33–36]. As observed for the $K_3[Ru(CN)_5(2-pyS-S)] \cdot 3H_2O$ complex, the frequencies of the $v(CN)_{ax}$ and $v(CN)_{eq}$ modes indicate the reduced state of the ruthenium metal center [16,17]. The bands observed at frequencies lower than 800 cm^{-1} are assigned [33–36] to the $\delta(CCS)$ and $\delta(CSC)$ vibrational modes of the 1,4-dt ligand. At 1004 cm^{-1} the band assigned [33–36] to the $v(CC)$ mode is observed. The vibrational modes associated with the $v(CH)$ and $\delta(CH_2)$ out- and in-plane vibrations are observed from 2900 to 3070 cm^{-1} and from 800 to 1600 cm^{-1}, respectively [33–36].

The SERS spectrum of the $[Ru(CN)_5(1,4-dt)]^{3-}$ complex adsorbed on gold presents an intensification of the $\delta(CH_2)$ modes of the 1,4-dt moiety, from 1000 to 1600 cm^{-1}, in relation to the vibrational modes of the cyanide groups. Based on surface selection rules [37], this result indicates that the 1,4-dt moiety is closer to the surface than the cyanide groups. Also the enhancement of these modes as well as the changes in the frequency and/or intensity of the CS bands observed by comparing the SERS and the normal Raman spectra from 250 to 800 cm^{-1} suggest a *gauche* orientation [38,39] of the 1,4-dt head group with the complex partially tilted in relation to the surface. Similar result was observed for the SAM formed with the $[Ru(CN-py)(NH_3)_4(1,4-dt)]^{2+}$ complex, where CNpy = 4-cyanopyridine, on gold [30].

2.6. Electroactivity of the SAMs

For the electrochemical study of cytochrome c (cyt c) metalloprotein, a heme-protein that plays an essential role in the mitochondrial electron-transport chain through the $Fe^{III/II}$ redox process, the orientation toward the surface as well as the protein conformation in its native state is of great importance for the molecular recognition. The degradative adsorption of cyt c on metallic surfaces or on a SAM is detected by shifts on the $E_{1/2}$ value which, for the native protein, is observed at 0.04 V vs Ag|AgCl|Cl [40]. By using Monte Carlo and molecular dynamics simulation approach, Zhou et al. [41] concluded that, for a satisfactorily molecular SAM-cyt c recognition, the desired protein orientation is perpendicular to the surface and that strongly charged surfaces will cause a larger conformational change and the loss of bioactivity. More recently, the $E_{1/2}$ values observed for the cyt c protein by using SAMs formed with the $[Ru(CN-py)(NH_3)_4(1,4-dt)]^{2+}$ and $[Ru(CNpy)(NH_3)_4(pyS)]^{2+}$ complexes, where pyS = 4-mercaptopyridine, are indicative of the native form [30]. The shape of the cyt c voltammograms, however, showed to be dependent on the complex conformation on surface. For the $[Ru(CNpy)(NH_3)_4(pyS)]^{2+}$ complex, which is *trans* in relation to the surface, a better cyt c response is observed. Thus, besides a negative charged end initially proposed by Jun et al. [42], these results suggest that a perpendicular orientation also seems to be a determinant factor.

In this work, the heterogeneous electron transfer (hET) reaction of the cyt c protein was only assessed by the SAMs formed with the $[Ru(CN)_5(1,4-dt)]^{3-}$ and $[Ru(CN)_5(asp)]^{3-}$ complexes on gold. By accounting for the fact that bare metallic surfaces are not able to assess the cyt c hET reaction [26,43], this result is indicative of the gold modification by the $[Ru(CN)_5(asp)]^{3-}$ complex. As previously described,
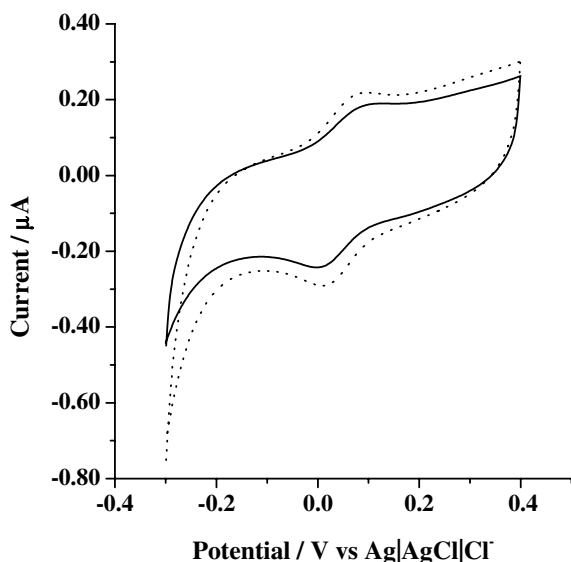
Fig. 4. Cyclic voltammograms at 50 mV s^{-1} of 0.1 mmol L^{-1} cyt *c* in 0.1 mol L^{-1} KH$_2$PO$_4$, pH = 7.0, for the gold electrodes modified with the [Ru(CN)$_5$(1,4-dt)]$^{3-}$ (solid line) and [Ru(CN)$_5$(asp)]$^{3-}$ (dot line) complexes.

SERS spectra were not acquired for this modified electrode. Fig. 4 illustrates the cyclic voltammograms obtained for the cyt *c* solution in physiological medium with gold electrodes modified after 15 min of immersion in a 20 mmol L^{-1} aqueous solution of the [Ru(CN)$_5$(1,4-dt)]$^{3-}$ and [Ru(CN)$_5$(asp)]$^{3-}$ complexes.

The cyclic voltammograms obtained with the modified electrodes present two redox waves assigned to the heme-Fe$^{III/II}$ redox process. The calculated $E_{1/2}$ values, ∼0.05 V, indicate the native state of the cyt *c* protein [40,42,43]. This result suggests that the SAMs formed by the [Ru(CN)$_5$(1,4-dt)]$^{3-}$ and [Ru(CN)$_5$(asp)]$^{3-}$ complexes avoid the cyt *c* degradative adsorption process on gold electrode. Additionally, the peak-to-peak potential separation for the reduction and oxidation processes was found to be ∼0.07 V indicating a rapid heterogeneous electron transfer kinetic.

By considering that charged surfaces and/or modifier conformations on surface may cause a loss of SAM electroactivity, the results presented in this work suggest that a negatively charged modifier seems to facilitate the assessment of the cyt *c* hET reaction more than the SAM conformation itself. This conclusion is based on the cyt *c* electrochemical response observed for the SAMs formed with the [Ru(CN)$_5$(1,4-dt)]$^{3-}$ and [Ru(CNpy)(NH$_3$)$_4$(1,4-dt)]$^{2+}$ [30] complexes. Although both compounds are *gauche* adsorbed on surface, as indicated by the SERS spectra, the cyclic voltammogram of the cyt *c* protein is better resolved for the [Ru(CN)$_5$(1,4-dt)]$^{3-}$ complex, which is negatively charged.

3. Conclusion

The results all together indicate that the 2-pySS ligand is coordinated to the [Ru(CN)$_5$]$^{3-}$ metal center through the

sulfur atom. As consequence, a strong stabilization of the ruthenium metal atom in the reduced state is observed based on the electrochemical results. Comparatively to systems in which the sixth ligand is a *N*-heterocyclic species, the stability enhancement is assigned to a relative stronger π-back-bonding interaction which involve the empty low-lying dπ orbitals of the sulfur atoms. The calculation of the negative electrostatic potential of the 2-pySS ligand indicates that the Lewis base centers are located on the sulfur atoms thus explaining the affinity of the soft Ru^{II} ion toward these atoms. This theoretical approach reinforces the experimental data obtained by cyclic voltammetry and vibrational and NMR spectroscopies.

SERS results showed that the [Ru(CN)$_5$(1,4-dt)]$^{3-}$ complex is adsorbed on gold through the sulfur atom of the 1,4-dt moiety. Additionally, the SERS spectra suggest a *gauche* conformation for this complex on surface. The cyt *c* hET reaction is assessed by the SAMs formed with the [Ru(CN)$_5$(1,4-dt)]$^{3-}$ and [Ru(CN)$_5$(asp)]$^{3-}$ complexes on gold. Based on the discussion presented in the literature since the 1970s, the modifier charge and conformation on surface are two of the most relevant aspects involved in the assessment of the cyt *c* hET reaction. By considering similar systems, the results presented in this work suggest that a negatively charged modifier facilitates the assessment of the cyt *c* hET reaction more than a *trans* conformation.

4. Experimental

4.1. Materials

The water used throughout was purified from a Milli-Q water system (Millipore Co.). Organic solvents were purified by standard procedures as described in the literature [44]. Potassium hexacyanoruthenate(II) trihydrate, K$_4$[Ru(CN)$_6$] · 3H$_2$O, was purchased from AlfaChemical Co., and the sulfur containing ligands, 1,4-dithiane, 2,2′-dithiodipyridine, and 2,2′-dithiodipyridine *N*-oxide were purchased from Aldrich. 2,6-dithiaspiro[3.3]heptane ligand was synthesized according to literature procedure [45]. Special care is required for this ligand and its complexes manipulation. It has a high toxicity and a very strong smell. For these reasons, all manipulations with this ligand and its complex were performed in laboratories by the use of glove box or in the hoods. Unfortunately, some important experimental data were not possible to be acquired to avoid the contamination of the laboratory.

Horse heart cytochrome *c* (type VI, 99%, Aldrich) was purified as described elsewhere [46]. All other reagents are of analytical grade.

4.2. Synthesis

K$_3$[Ru(CN)$_5$(L)] · 3H$_2$O type complexes, where L = 2,2′–dithiodipyridine (2-pySS) (1), 2,2′–dithiodipyridine *N*–oxide (2-pySSNO) (2), 1,4-dithiane (1,4-dt) (3), and 2,6-dithiaspiro[3.3]heptane (asp) (4) were synthesized according to

literature procedures for similar complex preparations [11], with minor modifications. A 47 mg (0.1 mmol) sample of $K_4[Ru(CN)_6] \cdot 3H_2O$ was dissolved in 5 mL of a 50% ethanol/water mixture followed by the addition of a Br_2 ethanol/water solution (0.10 mmolL^{-1}; 1 m molL^{-1} KBr), dropwise with stirring. After 20 min of reaction, an almost 3-fold excess (0.3 mmol) of the L ligand dissolved in 5 mL of ethanol was added dropwise, under a stream of argon. The resulting solution, which developed a yellow color for all ligands, was allowed to stand for 1 h to ensure complete reaction and cooled in an ice bath. Upon the slow addition of cold acetone, a yellow precipitate was obtained and collected by filtration, washed with acetone and ethyl ether, dried, and stored under vacuum in the absence of light. Anal. Calc.: (1) C, 28.93; H, 2.27; N, 15.74; S, 10.30. Found: C, 28.95; H, 2.31; N, 15.80; S, 10.19%. UV–Vis in aqueous solution: 270 and 340 nm ($\varepsilon = 1.0 \times 10^3$ L mol^{-1}cm^{-1}). (2) C, 26.38; H, 2.07; N, 18.47; S, 9.39 Found: C, 26.61; H, 2.10; N, 18.25; S, 9.48%. (3) C, 20.68; H, 2.70; N, 13.40; S, 12.27. Found: C, 20.45; H, 2.34; N, 13.28; S, 11.85%. (4) C, 22.46; H, 2.64; N, 13.10; S, 11.90. Found: C, 22.20; H, 2.45; N, 12.95; S, 11.85%. Yields were better than 80%. The complexes containing 2-pySSNO, 1,4-dt, and asp ligands were only synthesized aiming to correlate their electrochemical data with those obtained for the $[Ru(CN)_5$ (2-pySS)]$^{3-}$ complex. As can be seen in Chart 1, the 1,4-dt and asp ligands have only sulfur donor atoms whereas the 2-pySSNO ligand has its nitrogen atoms protected by the NO groups. Therefore, for these ligands, the sulfur atoms are the unique coordination sites.

4.3. Measurements

The elemental analyses were made at the Microanalysis Laboratory at the Institute of Chemistry at São Paulo University. ^{1}H NMR spectra, all of which made in D_2O solutions, were obtained on a T BRUKER DRX 400 spectrometer at 298 K. The 2,2-dimetyl-2-silapentane-5-sulfonate (DSS) compound was used as reference internal standard. Electronic spectra in the ultraviolet and visible (UV–Vis) regions were acquired with a Hitachi model U-2000 spectrophotometer. Chromatographic analyses were performed with a Shimadzu Liquid Chromatograph equipped with a model LC-10AD pump and an SPD-M10A UV–Vis photodiode-array detector with a CBM-10AD interface. An ODS column (250 mm × 4.6 mm i.d., 5 μm particles; from Altech) was used with an isocratic elution with 10:90 acetonitrile–water containing 0.1% HTFA, pH = 3.7. The chromatograms were taken at a constant flow-rate of 1.0 mL min^{-1}. Samples for analyses were dissolved in the mobile phase and 5 μL volumes were injected. The computational results presented were calculated with DMOL^3 within Material Studio 3.2 [47]. The transmission infrared spectra of the compounds dispersed in KBr were obtained by using a Perkin–Elmer instrument model Spectrum 1000. The vibrational Raman spectra were acquired by using a Renishaw Raman imaging microscope

system 3000 equipped with a CCD (charge-coupled device) detector, and an Olympus (BTH2) with a 50× objective to focus the laser beam on the sample in a backscattering configuration. As exciting radiation, λ_0, the 632.8 nm line from a He–Ne (Spectra-Physics) laser was used. Electrochemical experiments were performed with an electrochemical analyzer BAS 100 W from Bioanalytical System at 25 ± 0.2 °C. A conventional three-electrode glass cell with a glassy carbon ($A = 0.13$ cm^2 geometrical area) and a platinum foil were used as working and auxiliary electrodes, respectively, for the characterization of the complexes. For the cyt c electrochemical studies, polycrystalline gold surfaces ($A = 0.03$ cm^2 geometrical area) modified with the complexes were used as working electrode. The half-wave formal potentials ($E_{1/2}$) of the complexes and the cyt c were determined by cyclic voltammetry as the average value of the anodic (E_a) and cathodic (E_c) peak potentials. The polishing procedure of the gold surfaces was made as described by Qu et al. [48]. These electrodes were mechanically polished with alumina paste of different grade to a mirror finish, rinsed and sonicated (10 min) in Milli-Q water. The electrode was then immersed in a freshly prepared "piranha solution" (3:1 concentrated H_2SO_4/H_2O_2; **CAUTION**: Piranha solution is a high oxidant solution that reacts violently with organic compounds), rinsed exhaustively with water, and sonicated again. The cleanness was evaluated by comparison of the i–E curve obtained in a 0.5 M H_2SO_4 solution with the well-established one for a clean gold surface [49]. The surface modification procedure was made by immersing the gold electrodes in a 20 mmol L^{-1} aqueous solution of the complexes thus forming self-assembled monolayers (SAMs). All experimental procedures were performed at room temperature and the potentials cited throughout are quoted relative to an Ag|AgCl|Cl$^-$ (3.5 mmol L^{-1} KCl, BAS) reference electrode.

References

[1] C. Rovira, P. Carloni, M. Parrinello, J. Phys. Chem. B 103 (1999) 7031.
[2] A.L. Raphaels, H.B. Gray, J. Am. Chem. Soc. 113 (1991) 1038.
[3] S.J. Lippard, Acc. Chem. Res. 6 (1973) 282.
[4] C.G. Kuehn, S.S. Isied, Prog. Inorg. Chem. 27 (1979) 153.
[5] R.G. Pearson, J. Am. Chem. Soc. 85 (1963) 3533.
[6] H.E. Toma, A.A. Batista, H.B. Gray, J. Am. Chem. Soc. 104 (1982) 7509.
[7] J.W. Buchler, W. Kokisch, P.D. Smith, Struct. Bonding 34 (1978) 79.
[8] M.O. Santiago, J.R. Sousa, I.C.N. Diógenes, L.G.F. Lopes, E. Meyer, E. Castellano, J. Ellena, A.A. Batista, I.S. Moreira, Polyhedron 25 (2006) 1543.
[9] D.A. Buckingham, A.M. Sargeson, in: F.P. Dwyer, D.P. Mellor (Eds.), Chelating Agents and Metal Chelates, Academic Press, New York, 1964.
[10] H. Taube, in: A.F. Scott (Ed.), Survey of Progress in Chemistry, Academic Press, New York, 1973.
[11] I.S. Moreira, D.W. Franco, Inorg. Chem. 33 (1994) 1607.
[12] A. Ulman, Chem. Rev. 96 (1996) 1533.
[13] F.A. Kramer Jr., R. West, J. Phys. Chem. 69 (1965) 673.
[14] C.R. Johnson, R.E. Shepherd, Inorg. Chem. 22 (1983) 1117.
[15] K. Nakamoto, in: Infrared and Raman Spectra of Inorganic and Coordination Compounds, third ed., Wiley, New York, 1978.

[16] L. Tosi, Spectrochim. Acta 26 (1970) 1675.
[17] L. Tosi, Spectrochim. Acta 29 (1973) 353.
[18] D. Cook, Can. J. Chem. 39 (1961) 2009.
[19] J.H.S. Green, W. Kynaston, H.M. Paisley, Spectrochim. Acta 19 (1963) 549.
[20] K.H. Schmidt, A. Muller, Coord. Chem. Rev. 19 (1976) 41.
[21] A. Lautie, J. Hervieu, J. Beloc, Spectrochim. Acta 39A (1983) 367.
[22] J.H.S. Green, Spectrochim. Acta A 24 (1968) 1627.
[23] A.J. Bard, L.R. Faulkner, in: Electrochemical Methods, Fundamentals and Applications, Wiley, New York, 1980.
[24] S. Siddiqui, W.W. Henderson, R.E. Shepherd, Inorg. Chem. 26 (1987) 3101.
[25] C.R. Johnson, R.E. Shepherd, Inorg. Chem. 22 (1983) 2439.
[26] I.C.N. Diógenes, F.C. Nart, M.L.A. Temperini, I.S. Moreira, Inorg. Chem. 40 (2001) 4884.
[27] W.W. Henderson, R.E. Shepherd, Inorg. Chem. 24 (1985) 2398.
[28] A. Albert, G.B. Barlin, J. Chem. Soc. (1959) 2384.
[29] L.-C. Wang, R.J. Boyd, J. Chem. Phys. 90 (1989) 1083.
[30] S.O. Pinheiro, F.O.N. Silva, I.M.M. Carvalho, L.G.F. Lopes, M.L.A. Temperini, G.F.S. Andrade, I.S. Moreira, I.C.N. Diógenes, J. Braz. Chem. Soc. 17 (2006) 1594.
[31] I.C.N. Diógenes, I.M.M. Carvalho, E. Longhnotti, L.G.F. Lopes, M.L.A. Temperini, G.F.S. Andrade, I.S. Moreira, J. Electroanal. Chem. 605 (2007) 1.
[32] S.O. Pinheiro, J.R. Sousa, M.O. Santiago, I.M.M. Carvalho, A.L.R. Silva, A.A. Batista, E.E. Castellano, J. Ellena, I.S. Moreira, I.C.N. Diógenes, Inorg. Chim. Acta 359 (2006) 391.
[33] R.A. Walton, Inorg. Chem. 5 (1966) 643.
[34] P. Klaboe, Spectrochim. Acta A 25 (1969) 1437.
[35] G. Hagen, P. Klaboe, O.H. Ellestad, Spectrochim. Acta 28A (1972) 137.
[36] T.E. Rosso, M.W. Ellzy, J.O. Jensen, F. Hameka, D. Zeroka, Spectrochim. Acta A 55 (1999) 121.
[37] J.A. Creighton, in: R.J.H. Clark, R.E. Hester (Eds.), Selection Rules for Surface-Enhanced Raman Spectroscopy. Spectroscopy of Surfaces, Wiley, Chichester, 1988.
[38] M.A. Bryant, J.E. Pemberton, J. Am. Chem. Soc. 113 (1991) 3629.
[39] L.S. Wong, V.C. Vilker, W.T. Yap, V. Reipa, Langmuir 11 (1995) 4818.
[40] M.J. Eddowes, H.A.O. Hill, J. Am. Chem. Soc. 101 (1979) 4461.
[41] J. Zhou, J. Zheng, S. Jiang, J. Phys. Chem. B 108 (2004) 17418.
[42] F.K. Jun, I. Satake, K. Ueda, H. Akutsu, K. Niki, Redox Chem. Int. Behavior Biol. Mol. (1984) 125.
[43] F.A. Armstrong, Struct. Bonding 72 (1990) 137.
[44] D.D. Perrin, W.L.F. Amarengo, D.K. Perrin, in: Purification of Laboratory Chemicals, Pergamon Press, New York, 1980.
[45] G. Seitz, W.D. Mikulla, Tetrahedron Lett. 9 (1970) 615.
[46] D.L. Brautigan, M.S. Ferguson, E. Margoliash, Methods Enzymol. 53 (1978) 128.
[47] DMOL³ Module, MS Modeling Version 3.2; Accelrys Inc., San Diego, 2003.
[48] X. Qu, T. Lu, S. Dong, J. Mol. Catal. 102 (1995) 111.
[49] D.T. Sawyer, A. Sobkowiak, J.L. Roberts Jr., in: Electrochemistry for Chemists, 2nd ed., John Wiley & Sons, New York, 1995.